



Characterization of medieval-like glass alteration layers by laser spectroscopy and nonlinear optical microscopy

Mohamed Oujja^{1,a} , Teresa Palomar², Marina Martínez-Weinbaum¹,
Sagrario Martínez-Ramírez³, Marta Castillejo¹

¹ Instituto de Química Física Rocasolano, IQFR-CSIC, C/Serrano 119, 28006 Madrid, Spain

² Instituto de Cerámica y Vidrio, ICV-CSIC, C/Kelsen 5, Campus de Cantoblanco, 28049 Madrid, Spain

³ Instituto de Estructura de la Materia, IEM-CSIC, C/Serrano 121, 28006 Madrid, Spain

Received: 29 April 2021 / Accepted: 2 August 2021

© The Author(s) 2021

Abstract Historical glass-based objects undergo, since the time of their manufacture, different degradation phenomena that are related to their composition and to the environment to which they were exposed. Three-dimensional (3D) structural and chemical characterization of the degradation layers is important to select the most adequate conservation strategies for glass objects. Optical microscopy (OM) is the most frequently used non-destructive method to examine the surface of historical glasses; however, the 3D structural assessment of alteration layers requires applying the destructive modality of this technique to conduct a cross-sectional study. In this work, a different approach for structural and compositional characterization of alteration layers on model medieval-like glasses is presented, based on the combination of the laser spectroscopies of laser-induced breakdown spectroscopy (LIBS), laser-induced fluorescence (LIF) and FT-Raman, and the emerging, cutting edge technique of nonlinear optical microscopy (NLOM) in the modality of multiphoton excitation fluorescence (MPEF). The results obtained through this multi-analytical photonic approach were compared with those retrieved by examination of the surface and cross sections of the samples by OM and scanning electron microscopy–energy-dispersive X-ray spectroscopy (SEM–EDS). While the combination of LIBS, LIF and FT-Raman served to assess the composition of the various alteration layers, the use of MPEF microscopy allowed the non-destructive determination of the thicknesses of these layers, showing for both thickness and composition a good agreement with the OM and SEM–EDS results. Thus, the proposed approach, which avoids sample preparation, illustrates the capability of non-destructive, or micro-destructive in the case of LIBS, laser spectroscopies and microscopies for the in situ study of glass objects of historic or/and artistic value.

^a e-mail: m.oujja@iqfr.csic.es (corresponding author)

1 Introduction

Historical glasses are exposed to different alteration phenomena as a result of their interaction with the environment. They can be exposed to outdoor atmospheres, like in the case of stained glass windows, glass buildings or urban sculptures, to indoor atmospheres, as in a museum or a private collection, they can be submerged in a shipwreck, or, in the most common situation, buried in an archaeological site [1]. The degradation pathologies induced in historical glass objects depend on the aggressiveness of the alteration agents and on the time of exposure, but also on the chemical composition of the glasses.

The alteration mechanisms of glasses exposed to outdoor and indoor environments are controlled by rainwater and environmental humidity. These alteration agents induce the hydrolytic attack on the glass surface producing the lixiviation of alkaline and alkaline earth elements. The attack, or pitting, commonly appears isolated in different points of the surface; however, its growth can generate an interconnected continuous alteration layer [2–5]. The interaction of the lixivated alkaline and alkaline earth elements from the glass with the environmental gases (CO_2 , SO_2 , NO_x) can induce crystallization of salts on the glass surface and fissures inside the pits that could lead to their detachment [2, 3, 6]. In indoor atmospheres, glasses with non-equilibrated chemical compositions can be altered by exposure to environmental humidity and volatile organic acids, mainly formic and acetic acids. As a result, a continuous alteration layer is usually formed on the glass surface [7–10]. In dry atmospheres, this layer can appear fissured and even detached, leaving the inner glass core exposed to new alteration processes.

The glass pieces exposed to aquatic environments are mainly found in shipwrecks on the seabed [11]. They are fragments or whole objects commonly used during the trips, such as bowls, bottles and drinking glasses [11–14], or glass ingots and final trade products [15–18]. The degradation pathologies of these objects are directly dependent of the chemical composition of the glass, the time they were submerged and the presence of biofouling [11]. For Roman glasses with equilibrated chemical compositions, a multilayer structure is often observed, together with a thick continuous alteration layer in the most altered pieces, with a high content of alkaline elements [11].

Lastly, the historical glasses found in archaeological sites may have been exposed to burial environments during centuries [1]. The most common pathologies on buried glasses are multilayer crusts, pitting and deposits. The alteration layers are commonly formed as a consequence of the rain/drought cycles; however, the chemical characteristics of the soil (pH, ratios of textural fractions, organic matter, presence of carbonates, etc.) can directly affect their morphology [19, 20]. The presence of bubbles or inclusions in the glass network may favour localized alterations, forming pits in combination with the alteration crusts.

The conservation of historical glass objects is a crucial issue in the field of cultural heritage. The removal of weathering pathologies from an archaeological or historical glass is not a recommended practice as it could eliminate what is left from the original surface (superficial decorations or details of manufacturing) and the integrity of the remaining glass may be compromised [21]. In addition, the study of alteration layers can provide useful information about the environment to which the historical glass was exposed and provide clues about the most suitable conservation strategy to be adopted. Development of diagnostic and cleaning methods of historical glass objects benefits from accurate information related to composition of the body glass and of the degradation layers, and for the later, estimates of their thickness, preferably obtained in a way that does not compromise the integrity of the original glass object.

Different laboratory-based techniques are used for structural and compositional characterization of historical glasses. Glass alteration layers are traditionally studied by stereomicroscopy, conventional optical microscopy (OM) and scanning electron microscopy–energy-dispersive X-ray spectroscopy (SEM–EDS) [1, 22–24]. Stereomicroscopy allows to observe the morphology of surface alterations without sample preparation; however, OM in cross sections and SEM–EDS are destructive techniques that need sample preparation. Conventional X-ray fluorescence spectrometry (XRF), considered a destructive technique for which sampling and material preparation is required, is also applied in glass analysis [25]. Portable XRF devices are actually available for non-invasive *in situ* measurements, although they only allow superficial analysis due to the low X-ray penetration [26]. Infrared thermography (IRT) which detects the presence of alteration layers as a function of the different response from the glass surface and the altered layers to an induced heating effect is also considered standard analytical method for historical glass investigation [27, 28].

Laser-based techniques have become important tools for cultural heritage studies and in particular for analysing glass objects. Raman spectroscopy and Fourier transform infrared spectroscopy in attenuated total reflection mode (FTIR–ATR) serve to identify the presence of alteration layers based on the relative intensities of the stretching bands of Si–O–Si and Si–O[−] [29–32]. laser-induced breakdown spectroscopy (LIBS) and laser-induced fluorescence (LIF) are complementary techniques for the characterization of historical glasses. LIBS is micro-invasive and capable to determine the chemical elemental composition of historical glasses and alteration layers with stratigraphic capability [33–37]. On the other hand, LIF provides non-invasive superficial analytical information and facilitates the detection of trace elements and/or chromophores responsible of glass coloration [33, 38]. Another photonic method that serves to non-invasively measure the thickness of alteration layers is optical coherence tomography (OCT) based on the different light absorbance and scattering behaviour of transparent and translucent layers [39, 40]. In turn, fibre optics reflectance spectroscopy (FORS) enables the measurement of thickness of alteration layers according to changes in the intensity of bands of water overtones [41].

In the last years, cutting edge nonlinear optical microscopies (NLOM), using femtosecond lasers as light excitation sources, have been implemented in the field of cultural heritage as advanced tools for non-invasive 3D structural and chemical analysis [37, 38, 42–48]. As compared to traditional microscopy, NLOM offers several advantages associated with the intrinsic high-resolution three-dimensional sectioning capability. Femtosecond lasers induce various types of nonlinear optical responses due to their high peak power and short pulse duration and thus offer multimodal approaches for NLOM. After focusing with high numerical aperture objective lenses, the out-of-focus photobleaching- and photodegradation-induced phenomena are absent or minimal, thus ensuring the non-invasive character of the NLOM techniques.

Common NLOM modalities are multiphoton excitation fluorescence (MPEF) and second and third harmonic generation (SHG, THG). Specifically, MPEF provides 3D information with micrometric axial and lateral resolution on the chemical and structural composition of the sample [38, 42–47, 49]. In the case of historical glasses, MPEF has been successfully applied for non-invasive characterization of surface decorations (*grisailles*) on historical stained glass windows [37].

In this work, we have applied a set of photonic laser-based spectroscopies and MPEF microscopy for the structural and chemical characterization of artificial alteration layers on model medieval-like glasses. LIBS, LIF and micro-Raman spectroscopies were employed for the assessment of the elemental and molecular composition of the alteration layers, while MPEF allowed the non-invasive determination of the thickness of these layers. The results

obtained by examining cross sections by OM and SEM–EDS that provided thickness values and compositional information were compared with those retrieved with the above-mentioned photonic laser-based techniques. To the best of our knowledge, this is the first time that MPEF microscopy is used for the assessment of the thickness of alteration layers on medieval-like glass. The good agreement found for the two set of measurements exemplifies the possibility to carry out structural and chemical characterization of cultural heritage glass items in situ, in a non-destructive way and without sample preparation.

2 Materials and methods

2.1 Medieval-like model glass samples and alteration processes

The study was undertaken in medieval-like model glass samples subjected to various environmental and atmospheric conditions in order to generate alteration layers of different characteristics. A potash-lime silicate glass, with composition similar to that of medieval glasses, was melted at 1400 °C during two hours, poured in a brass mould of rectangular cross section and annealed at 650 °C. The resulting glass ingot was cut in slices of around $10 \times 10 \times 2 \text{ mm}^3$ and then polished using emery paper and an aqueous suspension of cerium oxide to obtain optical quality surfaces.

Alteration of the glass slices was conducted by exposure to five different laboratory corrosion tests. Figure 1 shows images of the unaltered medieval-like glass sample and of the samples generated by the induced alteration processes.

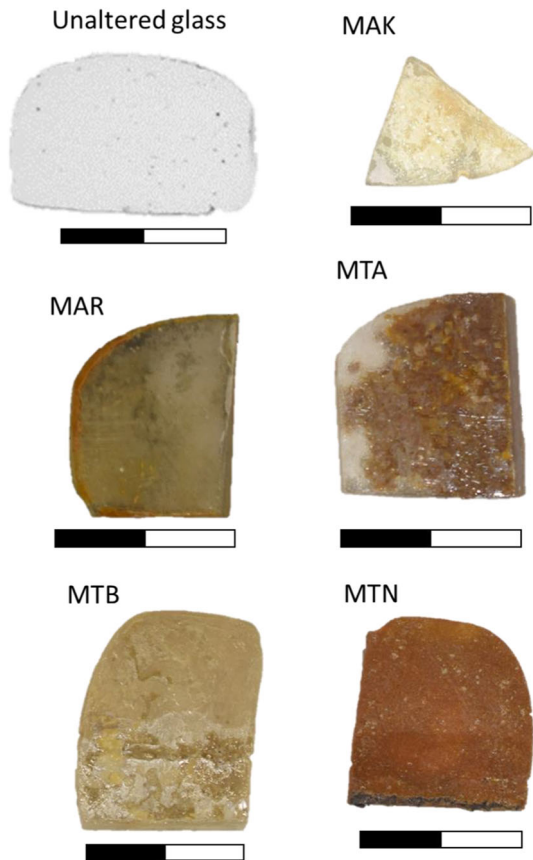
For the sample labelled MAK, a Kesternich VCK-300 corrosion chamber (Metrotec) was used following the standard DIN 50,018 (SO₂ corrosion) [50]. The glass sample was exposed to a 6667 ppm of SO₂ at 40 °C and 100% relative humidity (RH) during 8 h, followed by exposure to 16 h at environmental temperature, humidity and atmosphere. The test was repeated for five cycles. The sample named MAR was immersed in 25.0 ml of synthetic river water at 60 °C during 155 days [51]. Finally, three different accelerated ageing burial tests were carried out using acidic, neutral, and basic natural soils based on natural sand with pine spikes and/or topsoil [19]. The samples MTA (acidic), MTB (basic) and MTN (neutral) were buried in methacrylate boxes with a starting volume of soil of $65 \times 45 \times 13 \text{ mm}^3$ and 12.5 ml of distilled water. The burial tests were undertaken at 60 °C during 35 days. Every 5 days, 5.0 ml of distilled water was added to replace the evaporated water and maintain wet conditions [19].

2.2 Analytical methods

Glass samples were compositionally and structurally characterized by OM, SEM–EDS, LIBS, LIF and FT-Raman spectroscopy and by NLOM in the modality of MPEF.

A reflected light microscope Leica DM-LM with a Leica DFC 480 digital camera served for surface observation and thickness determination. The later was carried out on altered glass slices embedded into a polymeric resin and cut for cross-sectional observation. The SEM–EDS examinations were carried out with a Bruker AXS XFlash Quantax 4010 system, with an energy resolution of 125 eV (Mg K α), attached to a Hitachi microscope silicate S-3400-N, using acceleration voltages of 15 kV. The glass slices were observed during microanalyses on the polished cross sections inlaid into a polymeric resin and coated with carbon as conductive medium, using a Polaron SC7620 sputter coater (Hertfordshire, UK). EDS

Fig. 1 Images of unaltered medieval-like glass sample and of samples MAK, MAR, MTA, MTB and MTN resulting from exposure to different atmospheric and environmental conditions (see text). The measuring bar corresponds to 1 cm



determinations with the theoretical inner pattern were obtained by using the ZAF method of correction and the Bruker Sprit 1.8 analytical software.

LIB and LIF spectra were acquired upon laser excitation at 266 nm (4th harmonic of a Q-switched Nd:YAG laser, 15 ns pulses, 1 Hz repetition rate) and a 0.2 m spectrograph (Andor, Shamrock Kymera-193i-A) equipped with two gratings of 300 and 1200 grooves/mm, both blazed at 500 nm. The output of the spectrograph was coupled to an intensified charge-coupled device (ICCD) camera from Andor Technology (iStar CCD 334, 1024×1024 active pixels, $13 \mu\text{m} \times 13 \mu\text{m}$ pixel size). The laser beam for both techniques was conducted to the surface of the samples at the angle of 45° by using different mirrors. A cut-off filter of 300 nm was placed at the entrance slit of the spectrograph to reduce the scattered excitation laser light and to avoid the second-order diffraction. The shot-to-shot fluctuation of laser pulse energy was less than 10%. For LIBS, the laser beam was focused on the sample with a 10-cm focal length lens to reach a fluence of 8.3 J cm^{-2} (2.6 mJ per $200 \mu\text{m}$ laser spot diameter). The spectra were recorded using the spectrograph “step and glue” mode in the 300–600 nm wavelength range with 0.025 nm resolution and a temporal gate delay and width of 200 ns and 3 μs , respectively. For better distinguishing the composition of the degradation layers and of the unaltered glass body, LIB spectra corresponding to a single laser shot were recorded. In the case of LIF, the samples were illuminated through a pinhole, to select the central part of the unfocused laser beam, producing an elliptical laser spot shape with dimensions of $1 \text{ mm} \times$

2 mm. A fluence of around $6 \times 10^{-3} \text{ J/cm}^2$ (laser energy fixed at 0.1 mJ) was applied for recording the spectra. LIF spectra were also acquired in the “step and glue mode” in the wavelength range of 300–800 nm with a spectral resolution of 5 nm using the 300 lines/mm grating. LIF signals were collected with a time gate of 3 μs and zero-time delay with respect to the arrival of the laser pulse to the sample surface. Each LIF spectrum resulted from the accumulation of 10 individual ones.

The Raman spectra were collected with a Bruker FT-Raman MultiRam Spectrophotometer equipped with a cooled Ge detector. The excitation source consists of a continuous Nd:YAG laser emitting at 1064 nm. Before starting the acquisition of the FT-Raman spectra, several tests were performed with different laser powers and acquisition times on various sample areas. Spectra were collected on the same sample points several times so that the spectra were not modified by the effect of repetitive laser action. Controlled laser power output in the range of 200–300 mW was applied during measurements. The scattered light from an area of $<0.01 \text{ cm}^2$ was measured in the reflection geometry (180°). Each FT-Raman spectrum resulted from the accumulation of 200 scans with an exposure time and wavenumber resolution of 10 s and 4 cm^{-1} , respectively.

For MPEF studies, we used a home-made nonlinear optical microscope, described in detail elsewhere [37, 38, 44, 45], based on a mode-locked Ti:Sapphire femtosecond laser source. Briefly, the femtosecond laser emitting at 800 nm with an average power of 640 mW, pulse duration of 75 fs and a repetition rate of 80 MHz, was modulated by a chopper at a frequency of 130 Hz. The laser beam was conducted to the artificially altered glass samples through the aperture of a microscope objective lens (M Plan Apo HL 50X, Mitutoyo, NA of 0.42) by using a dichroic beam splitter (FF750-SDi02-25 \times 36, Semrock) with high reflection at 800 nm. The sample under study was placed on a motorized translation XYZ stage (with components Standa 8MVT100-25-1 for XY and Standa 8MTF for Z) that served to place the sample in the focal plane of the laser beam with lateral and axial resolutions of 1 and 2 μm , respectively. The MPEF signals generated from the volume of the sample situated in the focal plane of the objective lens were collected in the reflection mode after transmission through a beam splitter (70/30) and a cut-off filter, to reflect the remaining excitation laser light (short pass filter, 335–610 nm, Thorlabs FGB37S), and were measured with a photomultiplier tube (PMT, 9783B, ET Enterprises) connected to a lock-in amplifier (SR810 DSP, Stanford Research Systems) to ensure high amplification and signal-to-noise ratio. A LabVIEW interface served for control of the scanning and data acquisition procedures. The remaining 30% of the MPEF signal, after directing the remaining 70% to the PMT, was sent to a CCD camera (Thorlabs DCC1645C) for online visualization of the sample surface. During MPEF measurements the photon dose applied to the surface of the samples was 80×10^6 pulses/point.

The thickness value of the glass alteration layer was obtained by recording MPEF z-scan profiles in six different points of the sample surface. The full width at half maximum (FWHM) resulting from a Lorentzian function fitting of the profiles was then averaged and corrected by the apparent depth correction factor [37, 38]

$$F = \frac{1 - \sqrt{1 - \text{NA}^2}}{n - \sqrt{n^2 - \text{NA}^2}}$$

where NA is the numerical aperture of the focusing objective lens (0.42) and n the refractive index of the analysed material.

3 Results

The results presented in this work correspond to various measurements on different positions on the considered samples (altered and unaltered medieval-like glasses) using the analytical techniques indicated above. This was required to ensure the validity of the results obtained on samples with heterogeneous composition as those treated herein.

3.1 Optical microscopy and scanning electron microscopy/energy-dispersive X-ray spectroscopy

The surface and stratigraphy of the glass samples was studied by OM (Fig. 2) and their chemical composition determined by SEM–EDS (Table 1).

The chemical composition of the replica glass, as determined by SEM–EDS and indicated in Table 1, corresponds to that of a potash-lime silicate that is the typical, main compound of medieval-like glass.

The MAK sample, resulting from exposure to a SO₂-enriched atmosphere, shows a structure of five layers, in correspondence with the five alteration cycles applied (Fig. 2a). Each layer has a thickness of 6 to 9 μm with white crystals detected between layers that are probably due to the formation of sulphates. These crystals are generated in fissures of the altered layer due to the reaction of the environmental SO₂, dissolved in the adsorbed humidity, with the alkaline and alkaline earths leached from the glass core. Their growth favours the detachment of the most external layers giving rise to a quite heterogeneous crust (Fig. 2b). According with SEM–EDS measurements (Table 1), the alteration layer in this sample shows a high content of sulphur that could be related to the formation of calcium and potassium sulphates.

The MAR sample, generated by immersion in synthetic river water, displays a homogeneous surface with fissures and groups of circular pits (Fig. 2d). The pits have different sizes as a function of the degree of alteration, with depths between 25 and 55 μm (Fig. 2c). The altered layer has a single-layer homogenous profile, probably because the glass slice was permanently immersed in the aquatic environment. Circular fissures were observed around the pits, while the rest of the alteration layer shows a heterogeneous cracked surface as a result of the stresses between the altered and unaltered glass. In the area without pits, a homogeneous alteration layer of ~ 10 μm is observed. The chemical composition of the altered layer in cross section (Table 1) was depleted in potassium as result of the hydrolytic attack, although a relative increase of calcium and magnesium was observed. The presence of these elements, used as glass stabilizers, indicates that the aquatic medium only extracted the alkaline elements and not the alkaline earth ones.

The samples degraded in burial environments (MTA, MTB and MTN) showed fissured alteration layers (Fig. 2f, h, j) with a brownish hue. The sample MTA, buried in acidic soil, displays a multilayer structure of seven degradation layers, each 10–25 μm thick (Fig. 2e), where the most external ones appear partially detached as a consequence of their manipulation. Sandy material was observed between the most external layers. The chemical composition of the alteration layer (Table 1) showed the highest content of SiO₂ and the lowest content of K₂O of all samples studied because the acid pH of the environment favours the ion-exchange reaction between the potassium ions from the glass surface and the protons from the acidic soil [19].

The MTB sample, buried in basic soil, presented a thin alteration crust as result of the degradation and loss of the most external layers (Fig. 2h). The multilayered structure was less defined than in the MTA sample; however, at high magnification, layers of 5–10 μm thickness

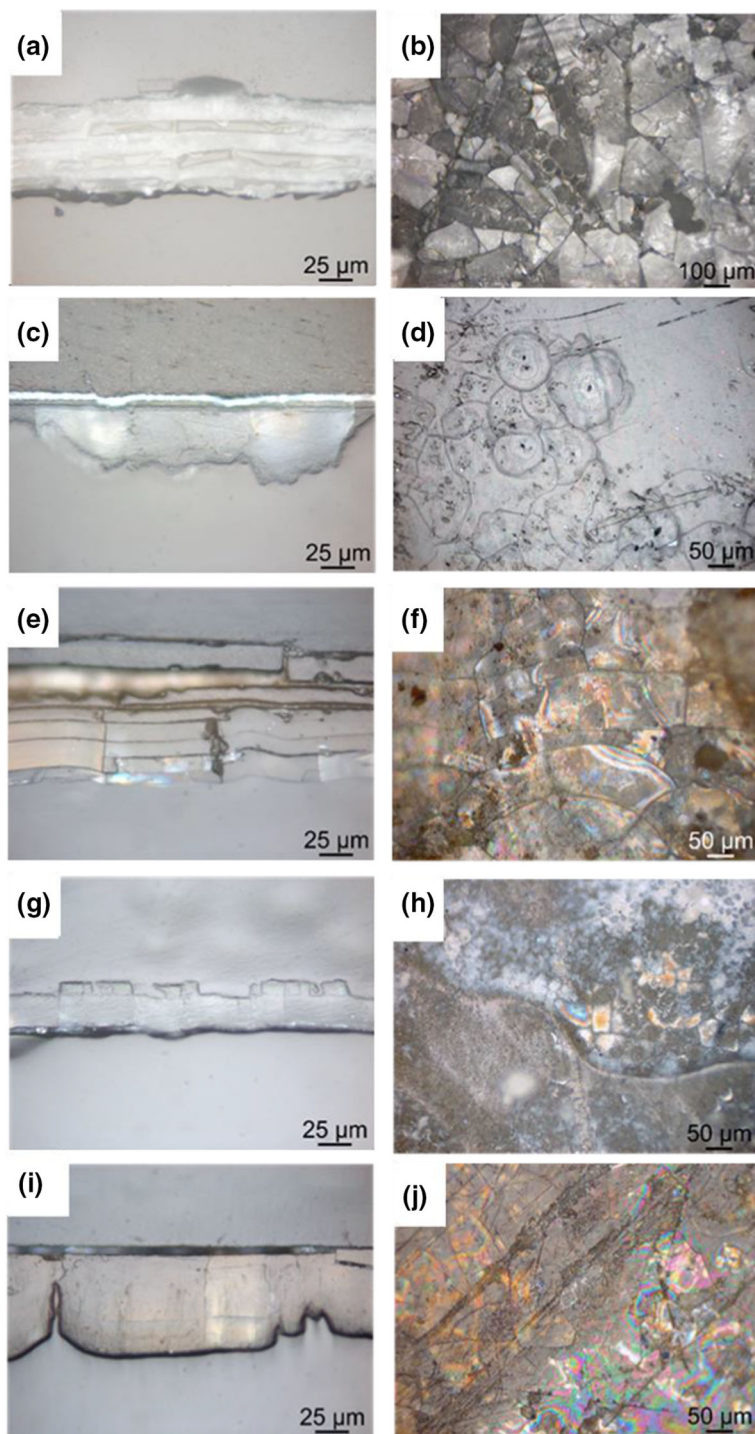


Fig. 2 Optical microscopy images of the surface (right column) and cross section (left column) of degradation layers on model medieval-like glass samples: **a, b** MAK; **c, d** MAR; **e, f** MTA; **g, h** MTB and **i, j** MTN

Table 1 Results (wt %) of SEM–EDS microanalyses carried out on the unaltered glass body and on the different degradation layers

Samples	Na ₂ O	MgO	Al ₂ O ₃	SiO ₂	P ₂ O ₅	SO ₂	Cl	K ₂ O	CaO	TiO ₂	MnO	Fe ₂ O ₃
Unaltered glass	1.3	3.3	3.1	37.2	3.3	–	–	24.6	27.2	–	–	–
MAK	0.1	–	2.3	43.7	1.8	22.6	0.2	3.2	26.1	–	–	–
MAR	–	5.2	3.3	44.1	3.7	0.4	0.1	2.1	41.1	–	–	–
MTA	0.9	0.9	8.1	74.1	3.5	–	–	1.7	9.2	–	1.0	0.5
MTB	4.1	10.4	16.1	60.1	0.9	0.8	0.6	5.0	1.9	0.1	–	–
MTN	1.0	0.9	9.7	53.1	9.0	–	–	2.4	24.0	–	–	–

–: Not detected

become evident (Fig. 2g). The basicity of the soil (pH~9) induced the loss of some alkaline and alkaline earth elements (Table 1). This high pH also induced a relative enrichment of MgO and Al₂O₃ in the corrosion crust.

Finally, the sample MTN shows a homogenous alteration layer as consequence of the neutral pH of the soil in which it was buried (Fig. 2j). Some irregularities were observed in the alteration front, probably as a consequence of inclusions or bubbles that could affect the hydration of the glass. The chemical composition of the alteration layer in this case shows a high content of CaO in comparison with the samples degraded in the other soils (Table 1). The presence of calcium indicates that the alteration conditions were not too aggressive to induce the loss of alkaline earth elements from the glass lattice, as in the MAR sample, and this could be the origin of the observed thick single-layer structure (Fig. 2i) observed in this sample.

The average values of the alteration layers in the MAK, MAR, MTA, MTB and MTN were measured in ten different locations along the cross section of the samples and estimated in average values of 58, 46, 97, 30 and 75 µm, respectively (see Sect. 3.5).

3.2 Laser-induced breakdown spectroscopy

Figure 3 displays LIB spectra recorded on the studied glass samples. The spectra revealed the presence of the main and minor elemental components by virtue of emission lines that were assigned based on data from the NIST database [52]. A summary of the elemental compositions retrieved from assignment of the LIBS emissions is presented in Table 2.

Figure 3a shows the LIB spectrum of the unaltered glass. Emission lines are assigned to aluminium (Al), calcium (Ca), magnesium (Mg), silicon (Si), potassium (K), strontium (Sr), barium (Ba), titanium (Ti), sodium (Na) and calcium oxide (CaO). K, Si and Ca constitute the main elements of the glass linked with the potash-lime silicate composition. The presence of other elements (Al, Mg, Sr, Ba, Ti and Na) was attributed to impurities from the glass raw material and/or stabilizing elements intentionally used in the glass manufacture. The LIB spectrum of the unaltered glass revealed the presence of a larger number of elemental components as compared with SEM–EDS (Table 1) indicating the high sensitivity of the former technique.

Lines of the main elements (K, Si and Ca) and of sodium were observed in the spectra of all analysed alteration layers with different intensities revealing different contributions of these elements. Particularly, the LIB spectra of samples MAK and MAR showed the presence of the same elements than in the unaltered glass, except for Ba and Sr in the former and Sr

Table 2 Elemental composition of model medieval-like glass and its corresponding degradation layers obtained by LIBS (The main components are indicated in bold)

Samples	Elemental composition
Unaltered glass	Al, Ca , Mg, Si, K , Sr, Ba, Ti, CaO , Na
MAK	Al, Ca , Mg, Si, K , Ti, CaO , Na
MAR	Al, Ca , Mg , Si, K, Ba, Ti, CaO , Na
MTA	Al, Ca , Mn , Fe, Mg, Si , K , Ba , Sr, Ti, CaO , Na
MTB	Al, Ca, Fe , Mg , Si , K , Sr, Ti, CaO, Na
MTN	Al, Ca, Mn , Mg, Si , K , Sr, Ba, Ti, CaO , Na

The LIB spectrum of the MTA sample, Fig. 3d, is similar to that of the unaltered glass, with the additional presence of manganese (Mn) and iron (Fe) lines. These elements are the responsible of the brown hue of this sample. A high content of silicon and barium, by virtue of their intense line emissions, has also been observed in this sample, possibly coming from the surrounding burial environment.

LIB spectra acquired on MTB and MTN samples were similar to the one recorded in the MTA sample, although in the former no Mn and Ba are observed, and in the later, lines of iron are absent. According with the intensity of the lines, MTB and MTN samples show a high content of Fe and Mn, respectively, responsible of the brown coloration of both samples. Mg line intensities are comparably high in the MTB sample, in agreement with the high content of this element as determined by SEM–EDS (Table 1).

LIBS analysis of the glass samples studied herein has revealed a high sensitivity for the detection of major and minor components of both the glass and of the alteration layers. Unlike SEM–EDS, that requires to prepare sample cross sections, LIBS is a micro-destructive technique. A comparison between the results obtained with these two elemental analysis techniques (Tables 1 and 2) indicates that through LIBS, it was possible to identify all sample elemental components in a micro-destructive way and that, even in some cases, elements that are difficult to determine by SEM–EDS are detectable by LIBS (trace elements, Na in low concentration, Boron). It should be noted that the elements P, S and Cl were undetectable by LIBS only because their main emission lines are outside the spectral range considered in this study (300–600 nm).

3.3 Laser-induced fluorescence spectroscopy

LIF spectra collected on the studied glass samples are displayed in Fig. 4. All spectra consist on a broad feature in the 300–800 nm region, although the different samples display special characteristics that are associated with their composition.

The spectra can be described as the sum of different contributions. In the region around 300–450 nm, a band with a shoulder at short wavelengths (330–360 nm) can be assigned, according to previous works [37, 53–55], to oxygen deficiency centres (ODC) from the glass network. The additional contribution centred in the region around 520 nm is attributed to the Ca^{2+} ion [56–58] present both in the glass lattice and in the burial media. The relative intensity of this feature is observed to increase with the calcium oxide content in the outer surface of each analysed sample, as revealed by LIBS and SEM–EDS.

The contribution of the feature associated to Ca^{2+} at 520 nm is substantial in the spectra of MAK and MAR samples (Fig. 4b, c). This is in correspondence with the significance of calcium sulphate and calcium carbonate bands, respectively, as revealed in their FT-Raman spectra (see Sect. 3.4) and the high content of Ca observed by SEM–EDS and LIBS.

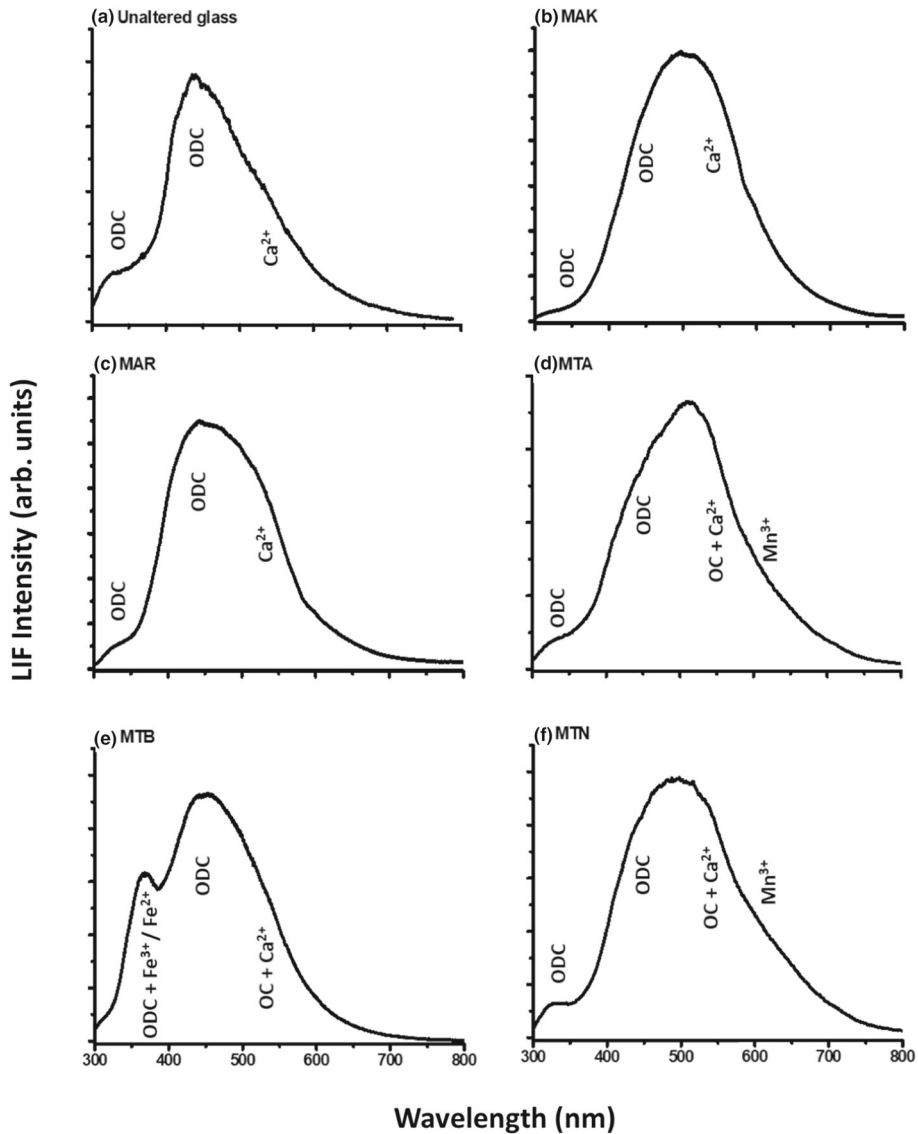


Fig. 4 LIF spectra of **a** the unaltered medieval-like glass and of the different degraded samples: **b** MAK; **c** MAR; **d** MTA; **e** MTB and **f** MTN. ODC and OC refer to bands due to oxygen deficiency centres and organic compounds, respectively. Each LIF spectrum resulted from the accumulation of ten individual ones upon laser excitation at 266 nm and using spectral resolution of 5 nm. Time delay and gate width were set to zero and 3 μ s, respectively

The spectra of samples MTA, MTB and MTN, while following the general trend of MAK and MAR spectra, display some specific additional features. For MTA, contributions in the spectral regions of 520 and 610 nm are assigned to bands of organic compounds with origin from the burial media consisting of natural sand with pine spikes and/or topsoil [59, 60], in addition to the Ca²⁺ contribution (as revealed by SEM-EDS and LIBS), and to the Mn³⁺

chromophore [33, 61], respectively (Fig. 4d). For the MTB sample (Fig. 4e), the prominence of the band at 360 nm, attributed to $\text{Fe}^{3+}/\text{Fe}^{2+}$ ions [33, 37], is related to the presence of iron oxides in the alteration layer, as revealed by LIBS and FT-Raman. Finally, the spectrum of the MTN sample (Fig. 4f) is similar to that of MTA with slight intensity variations in the regions around 450, 520 and 610 nm. The lower intensity in the 520 nm region in the LIF spectrum of this sample is in correspondence with the low intensity of bands of organic compounds observed by FT-Raman (Sect. 3.4).

Notwithstanding the relevance of the information about the composition of the glass alteration layers that is retrieved by assignment of the LIF spectra, it is important to note that, upon laser excitation at 266 nm, all samples analysed generate a broad emission in the spectral range that is used for collection of MPEF signals (335–610 nm). Excitation at 266 nm is equivalent to three-photon excitation of the sample atomic or molecular species at 800 nm, the wavelength of the femtosecond laser used in the NLOM setup of this study. This ensures that the MPEF signals that might be collected from the glass samples correspond to fluorescence emissions of the constituents of the analysed layers.

3.4 FT-Raman spectroscopy

The FT-Raman spectra of the medieval-like glasses are shown in Fig. 5. Figure 5a corresponds to the spectrum of the unaltered glass, where bands located in the wavenumber ranges of 500–700 and 750–1250 cm^{-1} are assigned to the bending and stretching modes of Si–O bonds, respectively, typically appearing in the twentieth-century stained silicate glasses ($\text{K}_2\text{O} + \text{CaO}$) [62, 63]. The structure of a silicate glass can be described in terms of the Q^n notation [64, 65], where n expresses the number of bonding oxygen (BO) atoms per tetrahedron: a tetrahedron fully linked into the network via four BO is labelled as a Q^4 unit, whereas an isolated tetrahedron with no BO corresponds to a Q^0 unit. The quantity of each of the five possible Q^n is used to describe the local structure and connectivity of the glass network. The stretching bands (in the range 750–1250 cm^{-1}) can be assigned in terms of Q^n to Q^0 (isolated SiO_4 between 750 and 850 cm^{-1}), Q^1 (900–950 cm^{-1}), Q^2 (990–1050 cm^{-1}), Q^3 (1100 cm^{-1}) and Q^4 (1150–1250 cm^{-1}). The bands at wavenumbers around 650 cm^{-1} correspond to the Si–O–Si bending massif modes for medieval-like glass. The above spectral features are generically indicated by the label MG in the FT-Raman spectra of the samples.

The spectrum of the MAK sample, subjected to SO_2 atmosphere (Fig. 5b), displays, together with the bands of the unaltered glass body, a doublet band with maxima at 1005 and 980 cm^{-1} , which together with the signals at 649, 620, 605, 489, 477, 448, 436 and 170 cm^{-1} allows the identification of calcium and potassium sulphate in the form of syngenite ($\text{K}_2\text{Ca}(\text{SO}_4)_2 \cdot \text{H}_2\text{O}$) [66].

Concerning the MAR sample, treated by immersion in synthetic river water (Fig. 5c), bands at 1085 and 289 cm^{-1} reveal the presence of calcium carbonate. Calcium carbonate can crystallize in three crystalline forms, calcite, aragonite and vaterite, with calcite being the most thermodynamically stable and therefore the most abundant. From the point of view of the vibrations of the three phases, the vaterite is clearly different, with signals at 1095, 1074, 740, 740 and 300 cm^{-1} . However, calcite and aragonite show a vibration at the same frequency, ν_1 1085 cm^{-1} , differentiated by the ν_4 and lattice vibrations at the wavenumbers around 712 and 280 cm^{-1} for calcite and around 705 and 205 cm^{-1} for aragonite [67]. Given the bands observed we can conclude that the spectra reveal the presence of calcite polymorph [68]. These results agree with those retrieved by SEM–EDS and LIBS (Tables 1 and 2).

Finally, Fig. 5d–f shows the FT-Raman spectra of MTA, MTB and MTN samples, respectively. Bands that were observed in the wavenumber range of 1200–2000 cm^{-1} are due to the

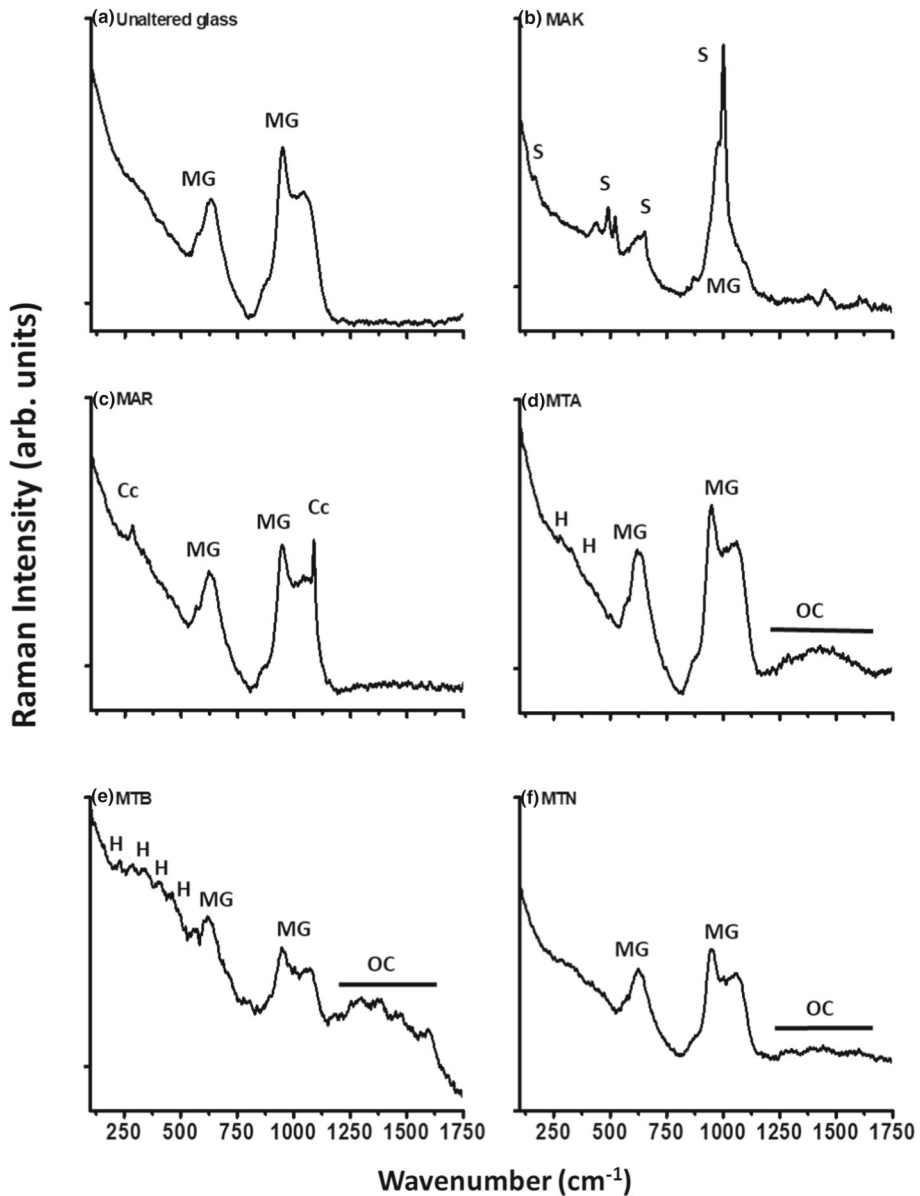


Fig. 5 FT-Raman spectra of unaltered medieval-like glass **a** and of degradation layers: **b** MAK; **c** MAR; **d** MTA; **e** MTB and **f** MTN. Spectral features labelled MG, S, Cc, H and OC correspond to bands assigned to the unaltered medieval-like glass (see text), calcium sulphate, calcite (calcium carbonate), hematite (Fe_2O_3) and organic compounds, respectively. Laser excitation and spectra resolution were 1064 nm and 4 cm^{-1} , respectively

vibrations of organic compounds present in the burial surrounding media where the samples were treated. Besides, in addition to the FT-Raman bands observed in the case of the unaltered glass, various bands at lower wavenumbers ($491, 402, 286$ and 220 cm^{-1}) appeared in the

spectra of MTA and MTB samples; these are attributed to a mixture of the iron (III) oxide (hematite, Fe_2O_3), clay and silica [69]. The iron was also observed by LIBS in the MTA and MTB samples with high intensity in the later in correspondence with FT-Raman results.

3.5 Multiphoton excitation fluorescence

In order to determine the thickness of the glass alteration layers via MPEF z-scan profiles under safe irradiation conditions, it is necessary to determine the suitable femtosecond average laser powers to ensure that the irradiated regions of the samples are not modified or damaged during measurements. To determine the adequate, safe operating laser powers, we used the procedure described in [44].

In short, the procedure consists in monitoring the variation of the intensity of the MPEF signal upon repetitive irradiation, as changes in intensity are a signature of possible structural or photochemical alteration of the irradiated area. To determine the onset laser power for modification or damage, the acquisition of MPEF signals is carried out by irradiating a certain point of the sample at a given laser power, then moving to a fresh area at increasing laser power and repeating the process until changes of intensity of the MPEF signals are detected. As shown in a previous work by some of us [44], the safe power limits are dependent of the irradiation mode (laser repetition rate, photon dose) and on the compositional characteristics of the sample.

In this work, to identify the adequate laser power limits for each glass sample, we collected four MPEF z-scan profiles in the same point of the sample at increasingly larger fixed laser powers in the range of 0.4–1.2 mW. Figure 6 displays a selection of the MPEF depth-scan profiles obtained in the various glass alteration layers. We observed different intensity trends according to the sample. The MPEF intensity increased upon repetitive irradiation cycles for MAK, MAR and MTB (Fig. 6a, c, g) and decreased for MTA and MTN samples (Fig. 6e, i). Applying the described procedure, safe average powers, where MPEF intensity is maintained upon the four cycles of irradiation, were estimated in 0.8, 0.6, 0.8, 0.8 and 0.65 mW for the samples MAK, MAR, MTA, MTB and MTN, respectively. MPEF z-scan profiles applying these safe average powers are presented in Fig. 6b, d, f, h, j where the stability of the signal becomes apparent.

Figure 7 shows an example of the MPEF z-scan profiles acquired on a random position of the samples by using the determined safe laser average powers. The thickness of the alteration layers on the medieval-like glasses were estimated, as indicated in Sect. 2.2, by measuring the full width at half maximum (FWHM) resulting from a Lorentzian function fitting of the MPEF profile and corrected by the F factor which depends of the material refractive index [38]. Refractive indices of medieval potash-lime stained glass samples were measured by A.A. Mills [70] and found to be in the range from 1.54 to 1.56. We assume that the average value of the refractive indices of the different alteration layers could only slightly deviate from that of the body glass and have estimated a value for F of 1.61. Table 3 compares the thickness of the various glass alteration layers as determined by MPEF and OM in the cross-sectional modality, where a general good agreement between the two sets of measurements is shown. It is to notice that the comparison is not entirely satisfactory for the MTA sample, a fact that could be related to the multilayer, inhomogeneous structure of its alteration layer (Fig. 2e).

As shown in Table 3, the thicknesses of the alteration layers depend on the nature of the surrounding exposure or burial conditions. The good agreement with OM results proves that MPEF microscopy is efficient to assess in a non-destructive way the variability in the thickness of the studied samples under safe measurement conditions.

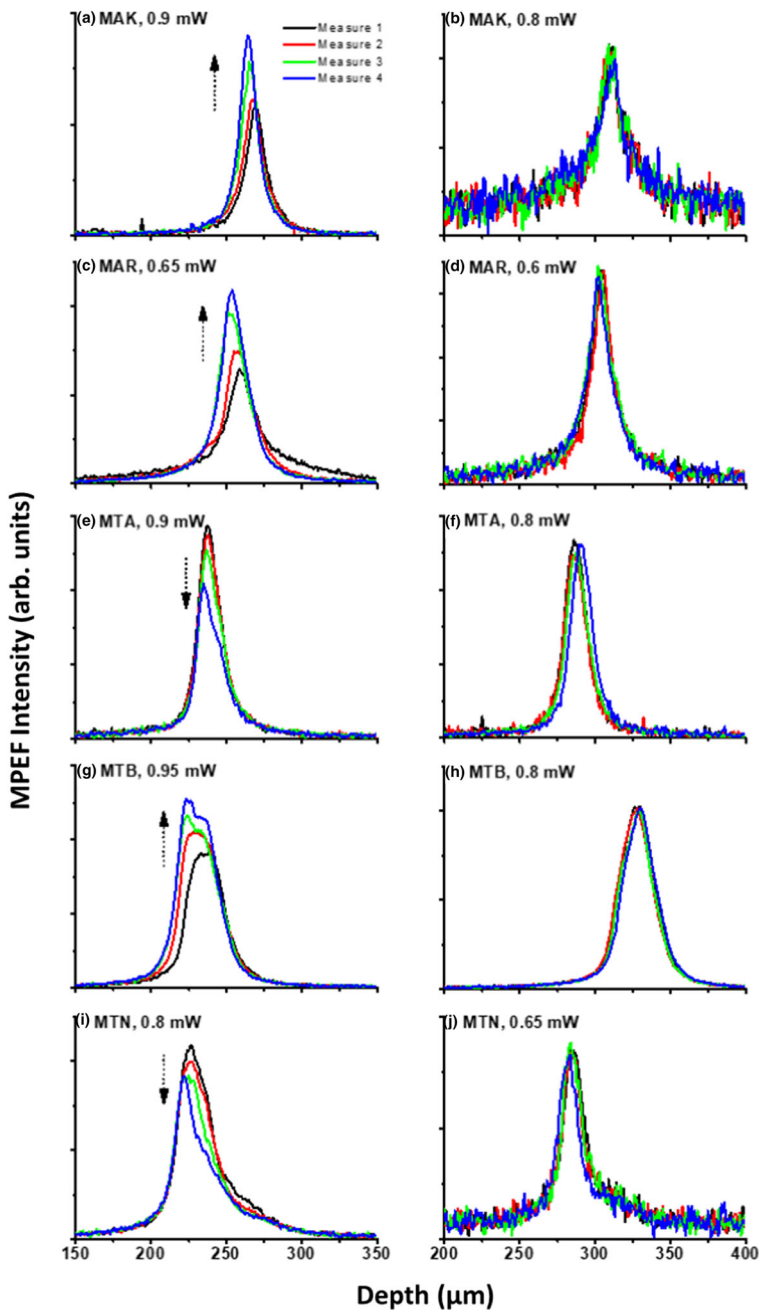


Fig. 6 Left column: MPEF depth-scan profiles of samples: **a** MAK, **c** MAR; **e** MTA; **g** MTB and **i** MTN at average laser powers of 0.9, 0.65, 0.9, 0.95 and 0.8 mW, respectively. As indicated by the arrows, the maximum fluorescence intensity at these laser powers tends to increase for MAK, MAR and MTB and to decrease for MTA and MTN samples as the number of axial scanning runs increases from 1 to 4. Right column: corresponding MPEF profiles using average laser powers of 0.8, 0.6, 0.8, 0.8, and 0.65 mW, considered suitable for safe analyses

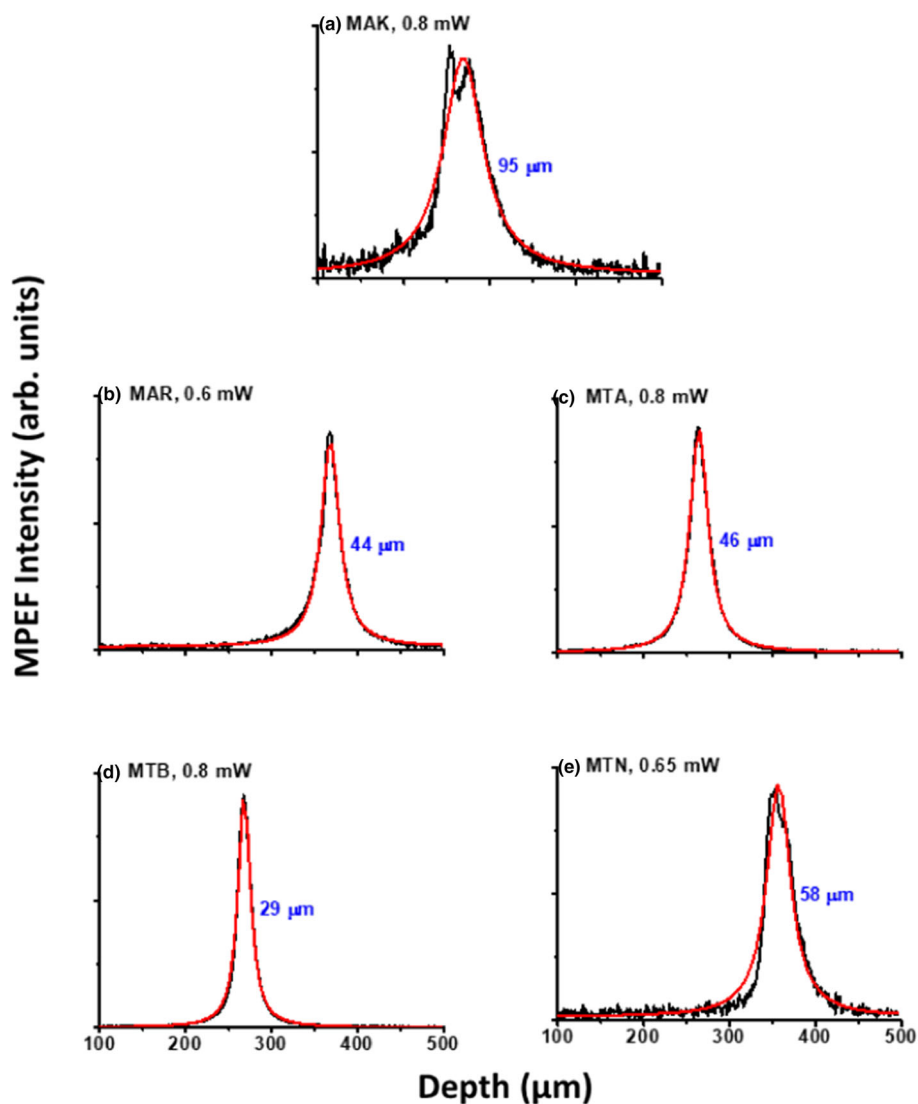


Fig. 7 Examples of MPEF z-scan profiles determined using safe laser average powers on random positions of the samples: **a** MAK; **b** MAR; **c** MTA; **d** MTB and **e** MTN. Fits with Lorentzian functions are indicated in red and the full width at half maximum (FWHM) values, after refractive index correction, in blue

4 Discussion and conclusions

The study presented in this manuscript has made use of the photonic laser-based spectroscopies of LIBS, LIF and FT-Raman for the determination of the elemental and molecular composition of model medieval-like glass and of different alteration layers. These layers were generated by exposure to different laboratory corrosion tests and mimic various usually encountered degradation pathologies in historic glasses. The manuscript also presents the capacity of MPEF microscopy to accurately determine in a non-invasive way the thickness

Table 3 Comparison between average thicknesses and standard deviation (in μm) of the alteration layers of model medieval-like glass samples as measured by OM in cross section and non-invasively by MPEF microscopy using previously determined safe average laser powers

Samples	OM	MPEF
MAK	58 ± 12	65 ± 18
MAR	46 ± 8	44 ± 12
MTA	97 ± 12	46 ± 10
MTB	30 ± 4	38 ± 8
MTN	75 ± 4	58 ± 16

of the glass degradation layers, an application of this technique never explored before. In the paragraphs below, we summarize the findings obtained by applying this photonic approach and compare them with those acquired by applying a more conventional, albeit destructive, characterization methodology based on OM and SEM–EDS.

LIBS allowed to determine the chemical nature of the glass matrix and of the artificial degradation layers, highlighting differences in their composition. The elemental composition of the unaltered medieval-like glass, consisting in Si, K and Ca, is compatible with that of a medieval-like potash-lime silicate. Other elements found, such as Al, Mg, Ba, Sr, Ti and Na, have their origin in the raw material and the stabilizing compounds used in the manufacturing process (Table 2). Alteration layers of samples MAK and MAR are, according to their LIB spectra, compositionally similar to the unaltered glass, although changes of intensity of emission lines indicate quantitative differences. For samples MTA, MTB and MTN, subjected to burial alteration environment, additional emission lines of Mn and Fe for MTA, of Fe for MTB and of Mn for MTN, testify the presence of compounds responsible of their brownish hue.

The elemental composition of both the glass matrix and the different artificial degradation layers was also identified by the invasive/destructive cross-sectional technique of SEM–EDS revealing the presence of similar components to those of medieval-like glass which mainly consist of potash-lime silicate glass. In addition to the main components Si, K and Ca, other elements were also detected, such as Mg, Na, Al and P which have their origin in impurities from the raw material and stabilizing agents used for glass manufacturing (Table 1). The MAK and MAR samples revealed different lixiviation processes of alkaline and alkaline earth elements from the glass lattice, with a high content of SO_2 and an increase in the calcium content, respectively. The SEM–EDS measurements carried out on the samples MTA, MTB and MTN showed also different lixiviation processes, as described previously in Sect. 3.1, with the presence of additional Ti, Mn, Fe, Cl and S from the burial surrounding media. SEM–EDS analysis gave the results (Table 1) that are in good agreement with those found by LIBS (Table 2). LIBS, a micro-destructive method, has revealed high sensitivity than other more established traditional analytical techniques used for elemental analysis of historical glasses (SEM–EDS, XRF, etc.). Moreover, the ability of LIBS to identify the presence of light and trace elements and chromophores, which yield valuable information on chronology, provenance and manufacturing process, adds extra value to the studies of historical glasses with this technique.

On the other hand, LIF has served for molecular assessment of the unaltered medieval-like glass matrix and their corresponding alteration layers. Spectra allowed to identify oxygen deficiency centres from the glass network, by virtue of bands around 350 and 450 nm. The emission at 520 nm indicate the presence of Ca^{2+} with origin in the compounds of the glass matrix and of the materials of the surrounding environments. LIF spectra of MTA and MTN

samples revealed the presence of the Mn^{3+} , through assignment of a band at 610 nm, while in the case of the MTB, iron compounds are apparent by the intense feature around 360 nm.

While LIF provided indications of the composition of the glass and of the alteration layers, FT-Raman spectroscopy facilitated its mineralogical identification. In fact, the FT-Raman bands observed for the unaltered glass allow classifying it as a $\text{K}_2\text{O} + \text{CaO}$ potash-lime silicate. The spectra of MAK and MAR samples revealed the respective presence of calcium and potassium sulphates originated by the exposure to an SO_2 atmosphere and of calcium carbonate associated with the effect of synthetic river water. Bands of organic compounds appear in the FT-Raman spectra of MTA, MTB and MTN samples, and of hematite in MTA and MTB samples, compound which is responsible of their brown coloration.

While LIF provided indications of the composition of the glass and of the alteration layers, FT-Raman spectroscopy facilitated its mineralogical identification. In fact, the FT-Raman bands observed for the unaltered glass allow classifying it as a $\text{K}_2\text{O} + \text{CaO}$ potash-lime silicate. The spectra of MAK and MAR samples revealed the respective presence of calcium and potassium sulphates originated by the exposure to an SO_2 atmosphere and of calcium carbonate due to the effect of synthetic river water. Bands of organic compounds appear in the FT-Raman spectra of MTA, MTB and MTN sample, and of hematite in MTA and MTB samples, the compound which is responsible of their brown coloration.

As seen, the combination of LIBS, LIF and FT-Raman spectroscopies provided a detailed chemical and mineralogical picture of the materials in the set of samples of this study. From this point of view, the complementary information gathered on the glass and the alteration layers by applying the three laser spectroscopies is perfectly compatible with the results concerning elemental composition obtained by SEM-EDS (summarized in Table 1). Apart from providing complete chemical information at elemental and molecular level, the obvious benefit of applying laser spectroscopies is indeed its non-destructive or micro-destructive character (as for LIBS) and their capacities for in situ analysis.

The photonic multi-analytical approach proposed here is complemented with the non-invasive, accurate determination of thickness of the alteration layers via MPEF microscopy. Through the determination of the adequate femtosecond laser powers that ensure safe measurement conditions, an accurate estimation of the thickness of glass degradation layers was possible via this technique, as confirmed through the comparison with the invasive OM technique in its cross-sectional modality (Table 3).

Thus, the methodology involving the application of photonic laser-based spectroscopies and nonlinear laser microscopy, exemplify the possibility to carry out a complete non-destructive or micro-destructive compositional and structural characterization of heritage glass items without sample preparation. The implementation of this approach in the field of cultural heritage and its application to real case studies in museums or in heritage building environments will come in hand with the ongoing advances in femtosecond laser technology and optical component arrangements that will facilitate the availability of robust, reliable and portable nonlinear optical microscopes integrating various NLO modalities.

Finally, given the results presented herein we consider that an approach based on the use of Raman spectroscopy and NLOM in the MPEF modality could constitute a valid, totally non-invasive methodology for a reliable determination of both the chemical composition and 3D structural arrangement of degradation layers, associated with exposure to different environments, in glass-based cultural heritage objects.

Acknowledgements This research has been funded by the Spanish State Research Agency (AEI) through projects PID2019-104124RB-I00/AEI/1013039/501100011033, the CSIC General Foundation (ComFuturo Programme), by project TOP Heritage-CM (S2018/NMT-4372) from Community of Madrid, by the H2020

European project IPERION HS (Integrated Platform for the European Research Infrastructure ON Heritage Science, GA 871034). Support by CSIC Interdisciplinary Platform “Open Heritage: Research and Society” (PTI-PAIS) is acknowledged. M.O. thanks CSIC for a contract. The authors also thank M.A. Villegas and M. García Heras (Institute of History, CSIC) for fruitful discussions on historical glasses.

Funding Open Access funding provided thanks to the CRUE-CSIC agreement with Springer Nature.

Declarations

Conflict of interest The authors declare no conflict of interest.

Open Access This article is licensed under a Creative Commons Attribution 4.0 International License, which permits use, sharing, adaptation, distribution and reproduction in any medium or format, as long as you give appropriate credit to the original author(s) and the source, provide a link to the Creative Commons licence, and indicate if changes were made. The images or other third party material in this article are included in the article's Creative Commons licence, unless indicated otherwise in a credit line to the material. If material is not included in the article's Creative Commons licence and your intended use is not permitted by statutory regulation or exceeds the permitted use, you will need to obtain permission directly from the copyright holder. To view a copy of this licence, visit <http://creativecommons.org/licenses/by/4.0/>.

References

1. T. Palomar, M. García-Heras, M.A.A. Villegas, Bol. Soc. Esp. Ceram. **48**, 187 (2009)
2. T. Palomar, Bol. Soc. Esp. Ceram. **57**, 101 (2018)
3. L. Gentaz, T. Lombardo, C. Loisel, A. Chabas, M. Vallotto, Environ. Sci. Pollut. Res. **18**, 291 (2011)
4. L. Sessegolo, A. Verney-Carron, P. Ausset, S. Nowak, S. Triquet, M. Saheb, A. Chabas, Chem. Geol. **550**, 119704 (2020)
5. M. Melcher, R. Wiesinger, M. Schreiner, Acc. Chem. Res. **43**, 916 (2010)
6. T. Lombardo, A. Ionescu, R.A. Lefèvre, A. Chabas, P. Ausset, H. Cachier, Atmos. Environ. **39**, 989 (2005)
7. J.J. Kunicki-Goldfinger, Stud. Conserv. **53**, 47 (2008)
8. T. Palomar, A. Rodrigues, Ge-Conservacion **17**, 226 (2020)
9. R. Arévalo, J. Mosa, M. Aparicio, T. Palomar, J. Non. Cryst. Solids **565**, 120854 (2021)
10. R.H. Brill, Stud. Conserv. **20**, 121 (1975)
11. T. Palomar, Mater. Chem. Phys. **214**, 391 (2018)
12. V.Z. Kralj, C. Beltrame, I. Miholjek, M. Ferri, Int. J. Naut. Archaeol. **45**, 42 (2016)
13. D. Elkin, A. Argüeso, M. Grosso, C. Murray, D. Vainstub, R. Bastida, V. Dellino-Musgrave, Int. J. Naut. Archaeol. **36**, 32 (2007)
14. A. Tripathi, Curr. Sci. **86**, 1246 (2004)
15. G.F. Bass, F.H. van Doorninck, Int. J. Naut. Archaeol. **7**, 119 (1978)
16. A. Anastasiades, L. Ellis, Stud. Conserv. **53**, 225 (2008)
17. K. Karklins, Int. J. Naut. Archaeol. **20**, 33 (1991)
18. C. León, T. Palomar, P. Pastor Rey de Viñas, Rev. Glas. **8**, 44 (2020)
19. T. Palomar, Int. J. Appl. Glas. Sci. **8**, 177 (2017)
20. G.A. Cox, B.A. Ford, J. Mater. Sci. **28**, 5637 (1993)
21. S.P. Koob, *Conservation and Care of Glass Objects* (Archetype Publications and The Corning Museum of Glass, Corning, New York, 2006)
22. R. Prochazka, J. Non. Cryst. Solids **353**, 2052 (2007)
23. O. Schalm, W. Anaf, J. Non. Cryst. Solids **442**, 1 (2016)
24. T. Lombardo, L. Gentaz, A. Verney-Carron, A. Chabas, C. Loisel, D. Neff, E. Leroy, Corros. Sci. **72**, 10 (2013)
25. G.A. Cox, A.M. Pollard, Archaeometry **19**, 45 (1977)
26. S. Liu, Q. Li, F. Gan, P. Zhang, X-Ray Spectrom. **40**, 364 (2011)
27. F. Micheletti, J. Orsilli, J. Melada, M. Gargano, N. Ludwig, L. Bonizzoni, Microchem. J. **153**, 104388 (2020)
28. J. Melada, N. Ludwig, F. Micheletti, J. Orsilli, M. Gargano, L. Bonizzoni, Proceedings of 15th International Workshop on Advanced Infrared Technology and Application Vol. 27, 5 (2019)

29. V. Comite, M. Andreoli, D. Atzei, D. Barca, M. Fantauzzi, M.F. La Russa, A. Rossi, V. Guglielmi, P. Fermo, *Appl. Sci.* **10**, 7523 (2020)
30. T. Palomar, D. de la Fuente, M. Morcillo, M. Alvarez de Buergo, M. Vilarigues, *Build. Environ.* **147**, 305 (2019)
31. A. Rodrigues, S. Fearn, M. Vilarigues, *Corros. Sci.* **145**, 249 (2018)
32. A. Rodrigues, S. Fearn, T. Palomar, M. Vilarigues, *Corros. Sci.* **143**, 362 (2018)
33. M. Oujja, M. Sanz, F. Agua, J.F. Conde, M. García-Heras, A. Dávila, P. Oñate, J. Sanguino, J.R. Vázquez De Aldana, P. Moreno, M.A. Villegas, M. Castillejo, *J. Anal. At. Spectrom.* **30**, 1590 (2015)
34. K. Muller, H. Stege, *Archaeometry* **45**, 421 (2003)
35. N. Carmona, M. Oujja, S. Gaspard, M. García-Heras, M.A. Villegas, M. Castillejo, *Spectrochim Acta Part B At. Spectrosc.* **62**, 94 (2007)
36. N. Carmona, M. Oujja, E. Rebollar, H. Römmich, M. Castillejo, *Spectrochim Acta Part B At. Spectrosc.* **60**, 1155 (2005)
37. M. Oujja, F. Agua, M. Sanz, D. Morales-Martin, M. García-Heras, M.A. Villegas, M. Castillejo, *Talanta* **230**, 122314 (2021)
38. A.D. Fovo, M. Oujja, M. Sanz, A. Martínez-Hernández, M.V. Cañamares, M. Castillejo, R. Fontana, *Spectrochim Acta Part A Mol. Biomol. Spectrosc.* **208**, 262 (2019)
39. L. Brostoff, C. L. Ward Bamford, T. Diba, A. Buechele, M. H. Loew, and J. M. Zara, in *Proc. SPIE - Opt. Arts, Archit. Archaeol. VII*, edited by P. Targowski, R. Groves, and H. Liang (SPIE, 2019), p. 31.
40. J. Kunicki-Goldfinger, P. Targowski, M. Góra, P. Karaszkievicz, P. Dzierzanowski, *Stud. Conserv.* **54**, 117 (2009)
41. S. Zaleski, E. Montagnino, L. Brostoff, I. Muller, A. Buechele, C. Lynn Ward-Bamford, F. France, M. Loew, *J. Am. Ceram. Soc.* **103**, 158 (2020)
42. G. Filippidis, G.J. Tserevelakis, A. Selimis, C. Fotakis, *Appl. Phys. A Mater. Sci. Process.* **118**, 417 (2015)
43. F. Faraldi, G.J. Tserevelakis, G. Filippidis, G.M. Ingo, C. Riccucci, C. Fotakis, *Appl. Phys. A Mater. Sci. Process.* **111**, 177 (2013)
44. A. Dal-Fovo, M. Sanz, S. Mattana, M. Oujja, M. Marchetti, F.S. Pavone, R. Cicchi, R. Fontana, M. Castillejo, *Microchem. J.* **154**, 104568 (2020)
45. A. Dal Fovo, M. Sanz, M. Oujja, R. Fontana, S. Mattana, R. Cicchi, P. Targowski, M. Sylwestrzak, A. Romani, C. Grazia, G. Filippidis, S. Psilodimitrakopoulos, A. Lemonis, M. Castillejo, *Sustainability* **12**, 3831 (2020)
46. H. Liang, M. Mari, C.S. Cheung, S. Kogou, P. Johnson, G. Filippidis, *Opt. Express* **25**, 19640 (2017)
47. G. Latour, J.-P. Echard, M. Didier, M.-C. Schanne-Klein, *Opt. Express* **20**, 24623 (2012)
48. M. Mari, G. Filippidis, *Sustainability* **12**, 1409 (2020)
49. M. Oujja, S. Psilodimitrakopoulos, E. Carrasco, M. Sanz, A. Philippidis, A. Selimis, P. Pouli, G. Filippidis, M. Castillejo, *Phys. Chem. Chem. Phys.* **19**, 22836 (2017)
50. DIN 50018. Testing in a saturated atmosphere in the presence of sulfur dioxide, *DIN 50018. Testing in a Saturated Atmosphere in the Presence of Sulfur Dioxide* (2013).
51. T. Palomar, I. Llorente, *J. Non. Cryst. Solids* **449**, 20 (2016)
52. NIST Atomic Spectra Database [Online] <http://physics.nist.gov/asd>, (n.d.).
53. L. Skuja, *J. Alloys Compd.* **239**, 16 (1996)
54. J. Fournier, J. Néauport, P. Grua, V. Jubera, E. Fargin, D. Talaga, S. Jouannigot, in *Phys. Procedia* (Elsevier B.V., 2010), pp. 39–43
55. M.A. Stevens-Kalceff, *Mineral. Mag.* **73**, 585 (2009)
56. H. Chen, J. Peng, L. Yu, H. Chen, M. Sun, Z. Sun, R. Ni, K.A. Alamry, H.M. Marwani, S. Wang, *J. Fluoresc.* **30**, 463 (2020)
57. M.B. Toffolo, G. Ricci, L. Caneve, I. Kaplan-Ashiri, *Sci. Rep.* **9**, 16170 (2019)
58. N. Yamashita, M. Taga, T. Kono, N. Yamashita, *Photoluminescence Prop Gypsum J. Mineral. Petrol. Sci.* **106**, 169 (2011)
59. D.M.B.P. Milori, H.V.A. Galeti, L. Martin-Neto, J. Dieckow, M. González-Pérez, C. Bayer, J. Salton, *Soil Sci. Soc. Am. J.* **70**, 57 (2006)
60. M. González Pérez, D. M. B. P. Milori, L. Martin Neto, L. Alberto Colnago, C. Otávio Antonio De, R. Severiano Berton, and W. Bettiol, *Sci. Agric* **63**, 269 (2006)
61. S. Boggs, D. Krinsley, S. Boggs, and D. Krinsley, in *Appl. Cathodoluminescence Imaging to Study Sediment. Rocks* (Cambridge University Press, 2009), pp. 109–133
62. L. De Ferri, D. Bersani, P. Colomban, P.P. Lottici, G. Simon, G. Vezzalini, *J. Raman Spectrosc.* **43**, 1817 (2012)
63. P. Colomban, A. Tournié, *J. Cult. Herit.* **8**, 242 (2007)
64. L. De Ferri, D. Bersani, A. Lorenzi, P.P. Lottici, G. Vezzalini, G. Simon, *J. Non. Cryst. Solids* **358**, 814 (2012)

65. P. Colombari, A. Tournie, L. Bellot-Gurlet, J. Raman Spectrosc. **37**, 841 (2006)
66. P. Vargas Jentzsch, R.M. Bolanz, V. Ciobota, B. Kampe, P. Rösch, J. Majzlan, J. Popp, Vib. Spectrosc. **61**, 206 (2012)
67. S. Martinez-Ramirez, S. Sanchez-Cortes, J.V. Garcia-Ramos, C. Domingo, C. Fortes, M.T. Blanco-Varela, Cem. Concr. Res. **33**, 2063 (2003)
68. A. Martínez-Hernández, M. Oujja, M. Sanz, E. Carrasco, V. Detalle, M. Castillejo, J. Cult. Herit. **32**, 1 (2018)
69. I.M. Bell, R.J.H. Clark, P.J. Gibbs, Spectrochim Acta Part A Mol. Biomol. Spectrosc. **53**, 2159 (1997)
70. A.A. Mills, Stud. Conserv. **32**, 122 (1987)